Chemical Engineering Journal 164 (2010) 49–55

Contents lists available at ScienceDirect

Chemical Engineering Journal

journal homepage: www.elsevier.com/locate/cej

Effect of environmental conditions on Pb(II) adsorption on β-MnO_2

Donglin Zhao[a,b], Xin Yang[a], Hui Zhang[a], Changlun Chen[a,*], Xiangke Wang[a,*]

[a] Key Laboratory of Novel Thin Film Solar Cells, Institute of Plasma Physics, Chinese Academy of Sciences, P.O. Box 1126, Hefei 230031, PR China
[b] School of Materials and Chemical Engineering, Anhui University of Architecture, Hefei 230601, PR China

ARTICLE INFO

Article history:
Received 12 June 2010
Received in revised form 5 August 2010
Accepted 5 August 2010

Keywords:
Pb(II)
Adsorption
β-MnO_2
Humic acid
Fulvic acid

ABSTRACT

In this study, the adsorption of Pb(II) on β-MnO_2 as a function of various environmental conditions such as contact time, pH, ionic strength, humic acid (HA)/fulvic acid (FA), and temperature was investigated using batch techniques. The results indicated that the adsorption of Pb(II) on β-MnO_2 was obviously dependent on pH but independent of ionic strength. The presence of HA/FA enhanced the adsorption of Pb(II) on β-MnO_2 at low pH, whereas reduced Pb(II) adsorption on β-MnO_2 at high pH. The kinetic adsorption of Pb(II) on β-MnO_2 can be well fitted by the pseudo-second-order rate equation. The thermodynamic parameters (ΔH°, ΔS°, and ΔG°) were also calculated from the temperature dependent adsorption isotherms, and the results suggested that the adsorption of Pb(II) on β-MnO_2 was a spontaneous and endothermic process. The adsorption of Pb(II) on β-MnO_2 was attributed to surface complexation rather than ion exchange.

1. Introduction

Metal (hydr)oxides such as iron, manganese (hydr)oxides may play a very important role in adsorptions of heavy metal ions, and surface adsorptions of heavy metal ions on the metal (hydr)oxides can dominate the fate and transport of heavy metal ions to a large extent [1–10]. Manganese oxides are poorly crystalline oxides which are generally found in manganese-rich coatings. In the natural environment, trace metals and radionuclides, such as Cr, Co, Ni, Cu, Zn, Pb and UO_2^{2+} [4–10], can strongly interact with manganese oxides. β-MnO_2 is one of the most important scavengers of trace metals in soil, sediments and rocks. Adsorption of metal ions by β-MnO_2 in aqueous phases is a critical process for the environmental application of β-MnO_2 in water treatment as well as for the environmental assessment of physicochemical behaviors of metal ions on β-MnO_2.

Natural organic matters such as humic acid (HA) and fulvic acid (FA) are well known to exert strong effect on the adsorption of heavy metal ions on clay minerals and oxides [3,4]. Humic substances (HSs) represent a major fraction of dissolved organic compounds which are widely present in environment. Whether HA or FA exerts an enhancing or reducing effect on heavy metal ion adsorptions strongly depends on the complex behavior of heavy metal ions with HA/FA in the ternary water–HS–mineral surface systems [3,4]. Most of the previous studies suggested that HSs promote the adsorption of heavy metal ions at low pH and reduce the adsorption at high pH [4,11–14,18]. The increase of adsorption is explained by the adsorption of HSs on the mineral surface followed by the interaction of heavy metal ions with surface adsorbed HSs, whereas the reduction adsorption is explained by the formation of soluble HS–metal ion complexes in solution, which stabilize metal ions in aqueous solution [3,4]. In our laboratory, the adsorptions of heavy metal ions on minerals in the absence/presence of HSs had been extensively studied [3,4,11–18]. However, the investigation about the effect of HSs on the adsorptions of heavy metal ions on manganese oxides is still scarce.

In this work, we studied the adsorption of Pb(II) on β-MnO_2 under various chemistry conditions. Pb(II) was selected as a model heavy metal ion because of its extensive existence in environment. The objectives of this work are: (1) to study the adsorption of Pb(II) on β-MnO_2 under various common conditions such as contact time, pH, ionic strength, HSs and temperature by using batch technique; (2) to determine the thermodynamic parameters (ΔH°, ΔS°, and ΔG°) of Pb(II) on β-MnO_2 from the temperature dependent adsorption isotherms; and (3) to presume the adsorption mechanism of Pb(II) on β-MnO_2 and to estimate the possible application of β-MnO_2 in wastewater disposal.

2. Experimental

2.1. Materials

All chemicals used in this experiment were purchased in analytical purity and used directly without any further purification. All the reagents were prepared with Milli-Q water. HA and FA were extracted from the soil of Hua-Jia county (Gansu province, China),

* Corresponding authors. Tel.: +86 551 5592788; fax: +86 551 5591310.
E-mail addresses: clchen@ipp.ac.cn (C. Chen), xkwang@ipp.ac.cn (X. Wang).

1385-8947/$ – see front matter © 2010 Elsevier B.V. All rights reserved.
doi:10.1016/j.cej.2010.08.014

and were characterized in detail in our earlier studies [18–20]. Cross-polarization magic angle spinning (CPMAS) ^{13}C NMR spectra of HA and FA were divided into four chemical shift regions, i.e., 0–50 ppm, 51–105 ppm, 106–160 ppm and 161–200 ppm. The four regions were referred to as aliphatic, carbohydrate, aromatic, and carboxyl regions. HA and FA have also been characterized as a suite of three discrete acids with pK_a values listed in Table S1. The concentrations of functional groups of HA and FA determined by fitting the potentiometric titration data using FITEQL 3.1 are given in Table S1. In addition, the weight-averaged molecular weights (M_w) of dissolved HA and FA are evaluated according to the method of Chin et al. [21], and the M_w values of dissolved HA and FA are calculated to be 2108 and 1364, respectively.

2.2. Preparation and characterization of β-MnO_2

β-MnO_2 was prepared according to the modified method described in detail in a previous study [22]. The surface functional groups were characterized by Fourier transform infrared spectroscopy (FT-IR). As a consequence of the disruption of Mn–O–Mn chains and partial leaching of Mn atom, formation of new hydroxyl groups and H_2O molecules are obviously found in β-MnO_2 by FT-IR analysis. The FT-IR spectrum of the MnO_2 sample is shown in Fig. 1. The two peaks at about 520 and 720 cm^{-1} arise from the stretching vibration of the Mn–O and Mn–O–Mn bonds [23,24]. The peak at 1600 cm^{-1} is assigned to the bending vibration of H_2O and OH^-, which implies that hydroxyl groups exist in the as-synthesized nanostructures. The broad peak at 3200–3600 cm^{-1} can be assigned to the stretching vibration of the water molecule and OH^- in the lattice. The peak at 1600 cm^{-1} is assigned to the bending vibration of H_2O and OH^-, which implies that hydroxyl groups exist in the as-synthesized nanostructures. Structural characterization of MnO_2 was carried out by powder X-ray diffraction (XRD) in a Scintag XDS-2000 diffractometer with Cu Kα radiation (λ = 1.5418 Å) operated at a voltage of 45 kV and current of 40 mA. The typical XRD pattern is shown in Fig. 2. All the reflection peaks can be indexed to a β-MnO_2 (JCPDS card 81-2261) phase. No peaks for other types or for amorphous MnO_2 are observed in the XRD pattern, indicating high purity and crystallinity of the final sample. The specific surface area was obtained to be 398.55 $m^2\ g^{-1}$ by the Brunauer–Emmett–Teller (BET) method.

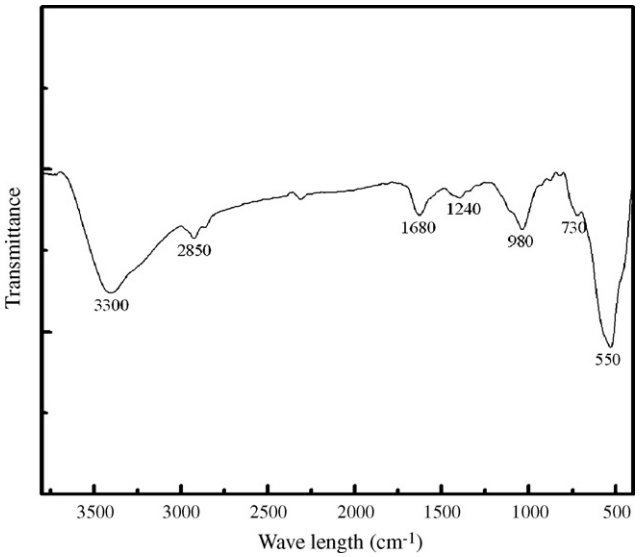

Fig. 1. FT-IR spectrum of β-MnO_2.

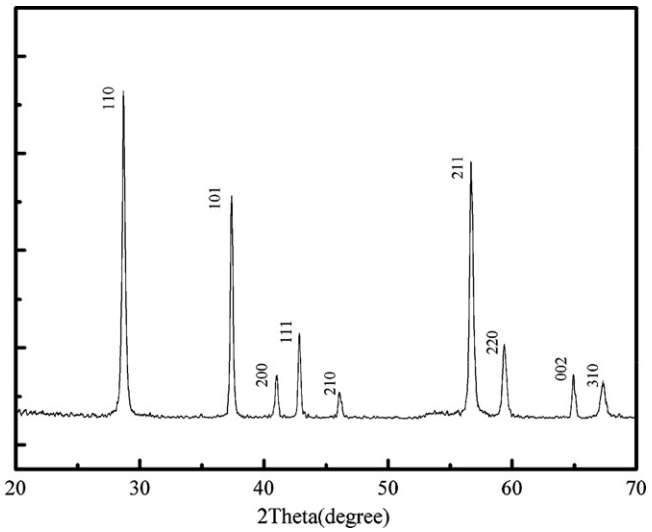

Fig. 2. XRD pattern of β-MnO_2.

2.3. Adsorption experiments

All the experiments were carried out at T = 293.15 K and under ambient conditions. The stock suspension of β-MnO_2, $NaClO_4$ solution, and Pb(II) stock solution were added into the polyethylene test tubes. As Pb(II) stock solution was prepared at pH ~ 3.5, a certain volume of 0.1 or 1.0 mol L^{-1} NaOH was added into the system to achieve the desired pH values and then the pH values of the systems were further adjusted by adding negligible volume of 0.1 or 0.01 mol L^{-1} $HClO_4$ or NaOH. After the suspensions were shaken for 24 h, the solid and liquid phases were separated by centrifugation at 9000 rpm for 30 min at the temperature controlled same to that in the adsorption experiments. It is enough to obtain the clear liquid phase.

The concentration of Pb(II) was analyzed using atomic absorption spectrophotometer. To take into account of Pb(II) loss from procedures except for β-MnO_2 adsorption (i.e., Pb(II) adsorption to tube wall), calibration curves were obtained separately under otherwise identical conditions as the adsorption process but no β-MnO_2. Based on the attained calibration curves, the amount of Pb(II) adsorbed on β-MnO_2 was calculated by subtracting the mass in the solution from the mass spiked. The adsorption of Pb(II) was expressed in terms of distribution coefficient (K_d) and adsorption (%), which were derived from Eqs. (1) and (2):

$$K_d = \frac{C_0 - C_e}{C_e}\frac{V}{m} \quad (1)$$

$$\text{Adsorption } (\%) = \frac{C_0 - C_e}{C_0} \times 100\% \quad (2)$$

where C_0 (mg L^{-1}) is the initial concentration, C_e (mg L^{-1}) is the concentration in supernatant after centrifugation, m (g) is the mass of β-MnO_2, and V (L) is the volume of the suspension.

All the experimental data were the averages of duplicate or triplicate experiments. The relative errors of the data were about 5%.

3. Results and discussion

3.1. Time-dependent adsorption

Fig. 3 shows the adsorption of Pb(II) on β-MnO_2 as a function of contact time. As can be seen from Fig. 3, the adsorption of Pb(II) on β-MnO_2 increases very quickly at the initial contact time, then the adsorption maintains high level with increasing contact time.

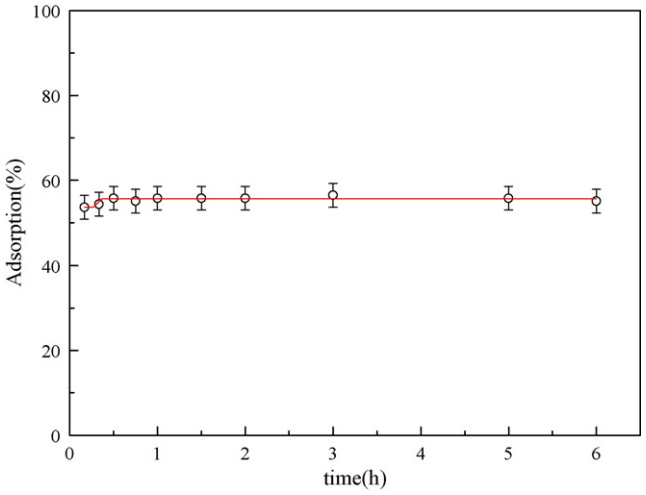

Fig. 3. Time dependent of Pb(II) adsorption on β-MnO_2, pH = 5.50 ± 0.02, T = 293.15 K, I = 0.01 mol L^{-1} $NaClO_4$, initial Pb(II) concentration = 10.0 mg L^{-1}, adsorbent content = 1.0 g L^{-1}.

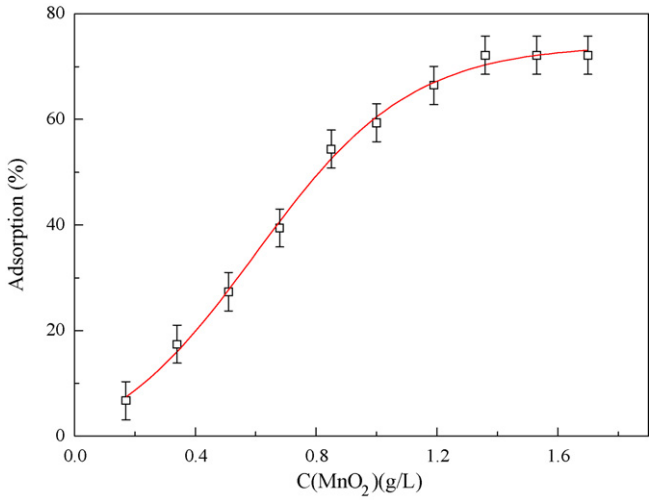

Fig. 4. Effect of β-MnO_2 content on Pb(II) adsorption on β-MnO_2, pH = 5.50 ± 0.02, T = 293.15 K, I = 0.01 mol L^{-1} $NaClO_4$, initial Pb(II) concentration = 10.0 mg L^{-1}.

The quick adsorption of Pb(II) on β-MnO_2 suggests that chemical adsorption rather than physical adsorption leads to Pb(II) adsorption on β-MnO_2 [25]. The results suggest that several hours is enough to achieve the equilibrium of adsorption of Pb(II) on β-MnO_2. According to the above results, the shaking time is fixed at 24 h in the following experiments to ensure that the adsorption reaction can achieve complete equilibrium.

In order to study the adsorption rate constant of Pb(II) on β-MnO_2, the pseudo-first-order and the pseudo-second-order rate equations were used to fit the kinetic adsorption of Pb(II) on β-MnO_2. From Fig. S1A and Table S2, the pseudo-first-order rate equation weakly fits the kinetic adsorption of Pb(II) on β-MnO_2. The pseudo-second-order rate equation is shown as follow [25]:

$$\frac{t}{q_t} = \frac{1}{2Kq_e^2} + \frac{1}{q_e}t \quad (3)$$

where q_t (mg g^{-1}) is the amount of Pb(II) adsorption on β-MnO_2 at contact time t (h), and q_e (mg g^{-1}) is the equilibrium adsorption capacity. K (g mg^{-1} h^{-1}) is the pseudo-second-order rate constant. A linear plot of t/q_t vs. t (Fig. S1B) was achieved, the correlation coefficients (R^2) of the pseudo-second-order rate equation for the linear plots is very close to 1, indicating that the kinetic adsorption of Pb(II) on β-MnO_2 can be well fitted by the pseudo-second-order rate equation.

3.2. Effect of solid content

The effect of β-MnO_2 content on the adsorption of Pb(II) on β-MnO_2 is shown in Fig. 4. The adsorption of Pb(II) from solution increases obviously with the increase in β-MnO_2 content at m/V < 1.0 g L^{-1}, and then increases very weakly with the increase in solid content at m/V > 1.0 g L^{-1}. As the β-MnO_2 content increases, the number of available sites for binding Pb(II) increases, which can enhance the removal of Pb(II) from solution to β-MnO_2 [3,4]. Sheng et al. [4] studied Ni(II) adsorption on MnO_2 as a function of solid content, and similar results were observed. This experimental phenomenon indicates that the augmentation of solid content could not unboundedly increase the contact area between metal ions and solid surface. Meanwhile, the competition adsorption between the adsorbent molecules will also reduce the adsorption quantity of solid particles. Thus, for the sake of reducing the cost of pollution management in actual application, one should choose appropriate adsorbent content according to the initial concentrations and required removal efficiency of the specific metal ions.

3.3. Effect of pH and ionic strength

In order to determine the pH effect on adsorption capacity of materials, solutions were prepared at different pH levels. Fig. 5 shows the adsorption of Pb(II) on β-MnO_2 by varying pH from 2 to 12 at 293.15 K in 0.1, 0.01 and 0.001 mol L^{-1} $NaClO_4$ solutions, respectively. The variation of pH in solution before and after adsorption has also been determined. The solution pH after adsorption changes a little to the acidic region, suggesting that H^+ is released during the adsorption process of Pb(II) on β-MnO_2. The adsorption of Pb(II) on β-MnO_2 increases at pH 2–7, maintains high level at pH 7–10, and then decreases sharply at pH > 10. Xu et al. [26,27] also reported the same phenomena of Pb(II) adsorption on bentonite and carbon nanotubes. The pH plays an important role in the adsorption of heavy metals ions on adsorbents. The pH changes in solution can affect the species distribution of metal ions in solution and the surface charge of the adsorbents via the dissociation of functional groups and change of surface charge, promoting or suppressing the adsorption of metal ions on adsorbent surface. Fig. S3 shows the acid–base titration data for β-MnO_2. At pH < 4.2, the surfaces were positively charged, and at pH > 4.2 the surfaces were negatively charged. The zero point of change (pH_{zpc}) is about 4.2. The increase of Pb(II) adsorption on β-MnO_2 with increas-

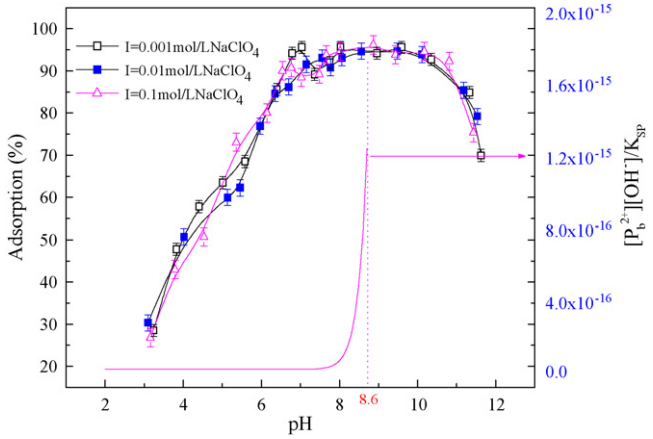

Fig. 5. Effect of ionic strength on Pb(II) adsorption on β-MnO_2 as a function of initial pH, adsorbent content = 1.0 g L^{-1}, initial Pb(II) concentration = 10.0 mg L^{-1}, T = 293.15 K.

ing solution pH may be attributed to the surface properties of β-MnO_2 in terms of surface charges and dissociation of functional groups. The surface of β-MnO_2 contains a large number of binding sites and may become positively charged at pH < 4.2 due to the protonation reaction on the surfaces (i.e., $SOH + H^+ \Leftrightarrow SOH_2^+$). The electrostatic repulsion occurred between Pb(II) ions and the edge groups with positive charge (SOH_2^+) on β-MnO_2 surface leads to the low adsorption efficiency of Pb(II). At pH > 4.2, the surface of β-MnO_2 becomes negatively charged due to the deprotonation process (i.e., $SOH \Leftrightarrow SO^- + H^+$) and electrostatic repulsion decreases with increasing pH due to the reduction of positive charge density on the adsorption edges, which enhances the adsorption of the positively charged Pb(II) ions through electrostatic force of attraction. The exact speciation of Pb(II) has a significant impact on the removal efficiency of β-MnO_2, thus the removal selectivity of Pb(II) by β-MnO_2 is influenced by the character of Pb(II) complex that predominates at a particular solution pH. Fig. S4 shows the relative distribution of Pb(II) species at ionic strength of 0.01 mol L^{-1} $NaClO_4$ from the hydrolysis constants ($\log k_1 = 6.48$, $\log k_2 = 11.16$, $\log k_3 = 14.16$) [28]. It is clear that Pb(II) species present in the forms of Pb^{2+}, $Pb(OH)^+$, $Pb(OH)_2^0$ and $Pb(OH)_3^-$ at various pH. The species of Pb(II) in solution at different pH values is most important for the removal of Pb(II) from aqueous solution to β-MnO_2. The precipitation constant of $Pb(OH)_2^0$ is 1.2×10^{-15}, and the precipitation curve of Pb(II) at the concentration of 10 mg L^{-1} is also shown in Fig. 5. From the precipitation curve, one can see that Pb(II) begins to form precipitation at pH ~ 8.6 if no Pb(II) is adsorbed on β-MnO_2. However, ~90% lead is adsorbed on β-MnO_2 at pH 7, and thereby at pH < 8.6, it is impossible to form precipitation because of the very low concentration of Pb(II) remained in solution. The adsorption of Pb(II) on β-MnO_2 at pH < 7 is not attributed to the precipitation of $Pb(OH)_2$. At pH < 7, the main species is Pb^{2+} and the removal of Pb^{2+} is mainly accomplished by adsorption. In the range of pH 7 ~ 10, the removal of Pb(II) reaches maximum and maintains high level. The main species at pH 7 ~ 10 are $Pb(OH)^+$ and $Pb(OH)_2^0$ and they can be easily adsorbed on the negatively charged β-MnO_2 surfaces. At pH > 10, the species of $Pb(OH)_3^-$ begin to form and the negative $Pb(OH)_3^-$ is difficult to be adsorbed on the negatively charged surfaces of β-MnO_2. From Fig. S4, at pH > 8.6, the part precipitation of $Pb(OH)_2$ may occur to some extent. According to the above analysis, the optimum pH range to adsorb Pb(II) from solution by using β-MnO_2 is from 7 to 8.6.

Fig. 5 also shows that the effect of ionic strength on Pb(II) adsorption to β-MnO_2 in the wide pH range is negligible. The results are consistent with those reported in the literatures [4,29–31]. Hayes and Leckie [32] have proposed that the effect of ionic strength on the adsorption can be used to predict the adsorption mechanism. β-Plane adsorption can occur when ionic strength easily affects the adsorption, otherwise, *o*-plane adsorption may occur. The results of this work suggest that Pb(II) participates in an *o*-plane complex reaction, without being affected by the β-plane complex reaction of ionic strength. The ionic strength independent adsorption and strongly pH dependent adsorption of Pb(II) on β-MnO_2 indicate that the adsorption mechanism of Pb(II) is surface complexation rather than ion exchange.

To illustrate the variation and relationship of pH, C_e, and q_e, herein, experimental data of Pb(II) adsorption in 0.1, 0.01 and 0.001 mol L^{-1} $NaClO_4$ were plotted as 3-D plots of pH, C_e, and q_e (see Fig. S5). On the pH–q_e plane, the lines are very similar to that of pH–adsorption percentage (in Fig. 5); On the pH–C_e plane, the projection on the pH–C_e plane is just the inverted image of the projection on the pH–q_e plane; On the C_e–q_e plane, the projection is a straight line containing all experimental data. It is obvious that the initial concentration of Pb(II) in each experimental point is the same. The following equation can describe the relationship of

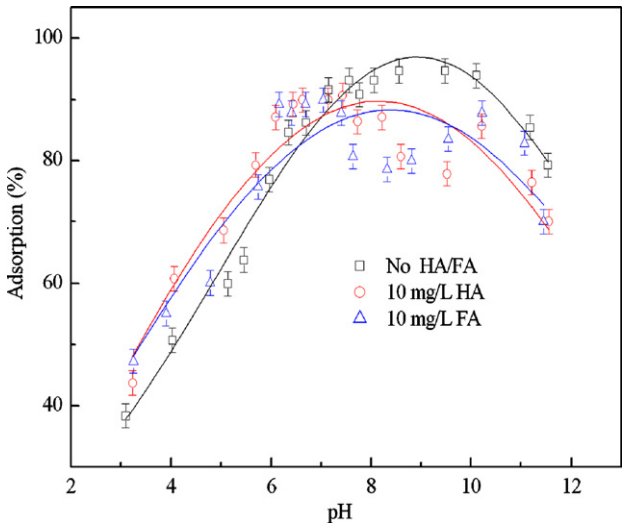

Fig. 6. Effect of HA/FA on the adsorption of Pb(II) on β-MnO_2 as a function of initial pH, adsorbent content = 1.0 g L^{-1}, initial Pb(II) concentration = 10.0 mg L^{-1}, I = 0.01 mol L^{-1} $NaClO_4$, T = 293.15 K.

C_e–q_e:

$$VC_0 = mq_e + VC_e \quad (4)$$

Eq. (4) can be rearranged as:

$$q_e = C_0\frac{V}{m} - C_e\frac{V}{m} \quad (5)$$

where V (L) is the volume of solution and m (g) is the mass of β-MnO_2. Thus, the experimental data of C_e–q_e lies in a straight line with a lope ($-V/m$) and intercept ($C_0 \cdot V/m$). The slope and intercept calculated from the C_e–q_e line are −1 and 10, which are quite in accordance with the values of $V/m = 1$ (L g^{-1}) and $C_0 \cdot V/m$=10 (mg L^{-1} L g^{-1}) (i.e., the values calculated from $V/m = 1$ L g^{-1} and $C_0 = 10$ mg L^{-1}). The 3-D plots show the relationship of pH, C_e, and q_e very clearly, i.e., all the data of C_e–q_e lie in a straight line with slope $-V/m$ and intercept $C_0 \cdot V/m$ for the same initial concentration of Pb(II) and the same β-MnO_2 content.

3.4. Effect of HA and FA

Fig. 6 shows the pH dependence of Pb(II) adsorption on β-MnO_2 in the absence and presence of HA/FA. The presence of HA/FA enhances the adsorption of Pb(II) on β-MnO_2 at pH < 7, while reduces Pb(II) adsorption at pH > 7. Fig. S6 shows the pH dependence of HA/FA adsorption on β-MnO_2. HA/FA adsorption on β-MnO_2 decrease from 85% to 20% with increasing pH from 2 to 10.5. HA/FA has a macromolecular structure, and only a small fraction of the "adsorbed" groups are free to interact with Pb(II) [3,4]. According to $\log K_a$ of dissociated HA/FA species, the distributions of surface site concentrations of HA/FA as a function of pH are shown in Fig. S7. The negatively charged species of HA/FA increase with a rise in pH. The complexation between Pb(II) and HA/FA is more stronger than that between Pb(II) and β-MnO_2. Besides, at low pH, the negatively charged HA/FA can be easily adsorbed on positively charged β-MnO_2, the strong complexation ability of surface adsorbed HA/FA with Pb(II) should enhance the adsorption of Pb(II) on β-MnO_2. With increasing pH, the negatively charged HA/FA is difficult to be adsorbed on negatively charged β-MnO_2. The free HA/FA forms soluble complexes of HA/FA–Pb(II) in solution, and therefore reduces Pb(II) adsorption on β-MnO_2. It is generally regarded that the presence of HA/FA promotes the adsorption of metal ions at low pH while declines the adsorption

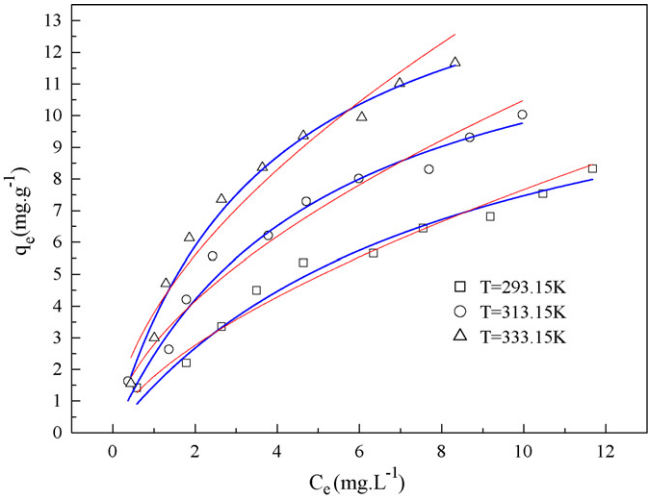

Fig. 7. Adsorption isotherms and the Langmuir, Freundlich models fitting for Pb(II) on β-MnO_2 at three different temperatures, adsorbent content = 1.0 g L^{-1}, pH = 5.50 ± 0.02, initial Pb(II) concentration = 2–20 mg L^{-1}, I = 0.01 mol L^{-1} $NaClO_4$. Symbols denote experimental data, solid lines represent the fitting of the Langmuir model equation and doted lines represent the fitting of the Freundlich model.

at high pH [33,34]. The results are similar to the effect of HA/FA on the adsorption of Ni(II) on goethite and Pb(II) on diatomite [3,15].

The adsorption curve of Pb(II) on β-MnO_2 in the presence of HA is quite similar to that in the presence of FA. The samples of HA and FA were extracted from the same soil samples, and thus they might have similar functional groups carboxyl groups, amine groups and phenolic groups. As is illustrated in Table S1, the quantitative concentrations of functional groups of HA are very similar to that of FA. These similar functional groups of HA and FA may interpret the similar adsorption curve of Pb(II) on β-MnO_2 in the presence of HA/FA.

3.5. Effect of temperature and thermodynamic data

The adsorption isotherms of Pb(II) on β-MnO_2 at 293.15, 313.15 and 333.15 K are shown in Fig. 7. One can see that the adsorption isotherm is the highest at 333.15 K and is the lowest at 293.15 K, indicating that the adsorption of Pb(II) on β-MnO_2 is promoted at higher temperature. One possible interpretation of this phenomenon is that Pb(II) ions are dissolved in water and the hydration sheaths of Pb(II) ions have to be destroyed before their adsorption on β-MnO_2 and this dehydration process needs energy, and that the adsorption of Pb(II) on β-MnO_2 gives off energy. The endothermic reaction exceeds the exothermic reaction and the result expresses endothermic process, so it is favored at high temperature [15].

The Langmuir model was first used to describe the adsorption of gas molecules onto a metal surface [35,36]. However, this model has been used successfully in many other processes. The form of the Langmuir isotherm can be represented by the following equation [35,34]:

$$q_e = \frac{bq_{\max}C_e}{1 + bC_e} \tag{6}$$

Eq. (6) can be expressed in linear form:

$$\frac{1}{q_e} = \frac{1}{q_{\max}} + \frac{1}{bq_{\max}} \cdot \frac{1}{C_e} \tag{7}$$

where C_e is the equilibrium concentration of Pb(II) remained in solution (mg L^{-1}), q_e is the amount of Pb(II) adsorbed per weight unit of solid after equilibrium (mg g^{-1}), $q_{\max}$ (maximum adsorption capacity) is the amount of Pb(II) at complete monolayer coverage (mg g^{-1}), and b (L g^{-1}) is a constant that relates to the heat of adsorption.

The Freundlich isotherm model allows for several kinds of adsorption sites on the solid surface and represents properly the adsorption data at low and intermediate concentrations on heterogeneous surfaces [35,37]. The model has the following form:

$$q_e = k_F C_e^n \tag{8}$$

Eq. (8) can be expressed in linear form:

$$\log\ q_e = \log\ k_F + n\ \log\ C_e \tag{9}$$

where k_F (mg^{1-n} g^{-1} L^n) represents the adsorption capacity when metal ion equilibrium concentration equals to 1, and n represents the degree of dependence of adsorption at equilibrium concentration.

The experimental data of Pb(II) adsorption on β-MnO_2 (Fig. 7) are regressively simulated with the Langmuir and Freundlich models and the results are given in Fig. S8. The related values calculated from the two models are listed in Table 1. One can conclude from fit curves shown in Fig. 7 and R^2 values and that the Langmuir model simulates the experimental data better than the Freundlich model. The fact that the adsorption data of Pb(II) according to the Langmuir isotherm indicates that the binding energy on the whole surface of β-MnO_2 is uniform. In other words, the whole surface has identical adsorption activity and therefore the interaction of adsorbed Pb(II) ions is negligible and Pb(II) ions are adsorbed by forming almost complete monolayer coverage of the β-MnO_2 particles [38]. Moreover, β-MnO_2 has a finite specific surface and adsorption capacity, thus the adsorption could be better described by the Langmuir model rather than by the Freundlich model, as an exponentially increasing adsorption was assumed in the Freundlich model.

The thermodynamic parameters (ΔH°, ΔS° and ΔG°) for Pb(II) adsorption on β-MnO_2 can be calculated from the temperature dependent adsorption isotherms. The values of standard enthalpy change (ΔH°) and standard entropy change (ΔS°) can be calculated from the slope and y-intercept of the plot of ln K_d vs. $1/T$ (Fig. S9) by applying the following equations:

$$\ln\ K_d = \frac{\Delta S^\circ}{R} - \frac{\Delta H^\circ}{RT} \tag{10}$$

where R (8.314 J mol^{-1} K^{-1}) is the ideal gas constant, and T (K) is the temperature in Kelvin.Free energy changes (ΔG°) is calculated from:

$$\Delta G^\circ = \Delta H^\circ - T\Delta S^\circ \tag{11}$$

The evaluation of thermodynamic parameters (see Table 2) provides an insight into the adsorption mechanism of Pb(II) on β-MnO_2. A positive value of the standard enthalpy change (ΔH°) indicates that the adsorption process is endothermic. The low value of ΔH° also suggests that the endothermic process of Pb(II) adsorption on β-MnO_2 is weak. As is expected for a spontaneous process under the experimental conditions, it is clear that the free energy changes (ΔG°) of Pb(II) adsorption on β-MnO_2 is more negative at higher temperature, which demonstrates that the spontaneity of the adsorption process increases with the rise in temperature. The positive value of entropy change (ΔS°) implies some structural changes in adsorbate and adsorbent during the adsorption process, which leads to an increase in the disorderness of the solid-solution system [39]. In principle, ΔH°, ΔS°, and ΔG° on basis of unite mass of reactants at a given temperature should be independent on the initial mass of reactants. From Table 2, it is worth to note that the obtained ΔH°, ΔS°, and ΔG° at variable initial Pb(II) concentrations are different. One possible interpretation was that in lower concentrations of Pb(II) ions, Pb(II) ions were completely solvated in water and Pb(II) ions were combined with more water molecules shown

Table 1
The parameters for Langmuir and Freundlich fitting of Pb(II) adsorption on MnO_2.

T (K)	Langmuir			Freundlich		
	q_{max} (mg g^{-1})	$1/b$ (L mg^{-1})	R^2	k_F (mg^{1-n} L^n g^{-1})	n	R^2
293.15	13.57	8.16	0.947	1.776	0.635	0.954
313.15	14.64	4.98	0.952	2.784	0.576	0.924
333.15	16.72	3.69	0.972	3.778	0.567	0.932

Table 2
Thermodynamic parameters for the adsorption of Pb(II) on MnO_2.

C_0 (mg L^{-1})	ΔH° (kJ mol^{-1})	ΔS° (J mol^{-1} K^{-1})	ΔG° (kJ mol^{-1})		
			293.15 K	313.15 K	333.15 K
8	19.13	124.94	−17.50	−19.99	−22.50
12	19.21	122.11	−16.58	−19.03	−21.47
14	17.44	115.56	−16.44	−18.75	−20.96
16	16.05	109.55	−16.06	−18.25	−20.44

in Fig. S10A, and in order for Pb(II) ions to adsorb, the dehydration sheath process of Pb(II) ions needed more energy. However, in higher concentrations of Pb(II) ions, Pb(II) ions were partly solvated in water and Pb(II) ions were combined with less water molecules shown in Fig. S10B, and the dehydration sheath process of Pb(II) ions needed less energy. Therefore, the obtained values of ΔH°, ΔS°, and ΔG° at variable initial Pb(II) concentrations are different, especially in the case of higher initial Pb(II) concentrations.

3.6. Regeneration

The repeated availability of β-MnO_2 for Pb(II) removal through many cycles of adsorption/desorption is quite crucial for the application of β-MnO_2 in the removal of Pb(II) from wastewater in real work [15]. Herein, the recycling of β-MnO_2 in the removal of Pb(II) was investigated. After adsorption, desorption was carried out by washing out β-MnO_2 adsorbed Pb(II) with acetic acid and Milli-Q water, then β-MnO_2 was dried at 75 °C. We found that the recycling was valid for at least five times shown in Fig. 8 to give a satisfied removal percentage even in the fifth round. This result suggests that β-MnO_2 can be employed repeatedly in Pb(II) adsorption.

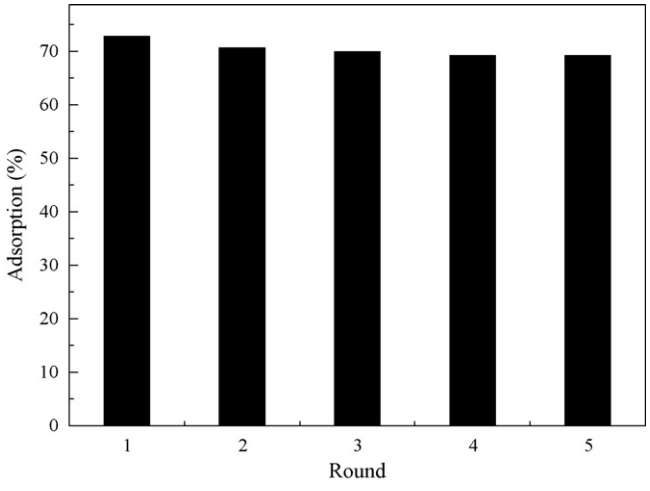

Fig. 8. Recycling of β-MnO_2 for the removal of Pb(II), adsorbent content = 1.0 g L^{-1}, pH = 5.50 ± 0.02, initial Pb(II) concentration = 10.0 mg L^{-1}, I = 0.01 mol L^{-1} $NaClO_4$.

4. Conclusions

From the results of Pb(II) adsorption on β-MnO_2 under our experimental conditions, the following conclusions can be obtained:

(1) The adsorption of Pb(II) on β-MnO_2 is rather quick and the kinetic adsorption is fitted by the pseudo-second-order model very well.
(2) The adsorption of Pb(II) on β-MnO_2 is dependent on pH but independent of ionic strength in a wide pH range. The adsorption of Pb(II) on β-MnO_2 is mainly dominated by surface complexation.
(3) The presence of HA/FA enhances the adsorption of Pb(II) on β-MnO_2 at low pH, while inhibits Pb(II) adsorption at high pH.
(4) The thermodynamic analysis derived from temperature dependent adsorption isotherms indicates that the adsorption reaction of Pb(II) on β-MnO_2 is endothermic and spontaneous.

Acknowledgement

Financial supports from the National Natural Science Foundation of China (20907055 and 20971126), 973 projects (2007CB936602), the Knowledge Innovation Program of CAS and Special Foundation for High-level Waste Disposal (2007-840) are acknowledged.

Appendix A. Supplementary data

Supplementary data associated with this article can be found, in the online version, at doi:10.1016/j.cej.2010.08.014.

References

[1] J. Gimenez, M. Martınez, J. Pablo, M. Rovira, L. Duro, Arsenic sorption onto natural hematite, magnetite, and goethite, J. Hazard. Mater. 141 (2007) 575–580.
[2] M. Rovira, J. Gimenez, M. Martınez, X. Martınez-Llado, J. Pablo, V. Martı, L. Duro, Sorption of selenium(IV) and selenium(VI) onto natural iron oxides: Goethite and hematite, J. Hazard. Mater. 150 (2008) 279–284.
[3] B. Hu, W. Cheng, H. Zhang, G. Sheng, Sorption of radionickel to goethite: effect of water quality parameters and temperature, J. Radioanal. Nucl. Chem. 285 (2010) 389–398.
[4] G. Sheng, J. Hu, H. Jin, S. Yang, X. Ren, J. Li, Y. Chen, X. Wang, Effect of humic acid, fulvic acid, pH, ionic strength and temperature on ^{63}Ni(II) sorption to MnO_2, Radiochim. Acta 98 (1–9) (2010) 1718, doi:10.1524/ract.2010.1718.

[5] R. Han, L. Zhu, W. Zou, D. Wang, J. Shi, J. Yang, Removal of copper(II) and lead(II) from aqueous solution by manganese oxide coated sand II. Equilibrium study and competitive adsorption, J. Hazard. Mater. B 137 (2006) 480–488.
[6] H. Tamura, N. Katayama, R. Furrich, The Co^{2+} adsorption properties of Al_2O_3, Fe_2O_3, Fe_3O_4, TiO_2, and MnO_2 evaluated by modeling with the Frumkin isotherm, J Colloid Interface Sci. 195 (1997) 192–202.
[7] J. Catts, D. Langmuir, Adsorption of Cu, Pb, and Zn by γ-MnO_2: applicability of the side binding-surface complexation model, Appl. Geochem. 1 (1986) 255–264.
[8] S. Kanungo, K. Paroda, Interfacial behavior of some synthetic MnO_2 samples during their adsorption of Cu^{2+} and Ba^{2+} from aqueous solution at 300 K, J. Colloid Interface Sci. 98 (1984) 252–260.
[9] M. Zaman, S. Mustafaa, S. Khan, B. Xing, Effect of phosphate complexation on Cd^{2+} sorption by manganese dioxide (β-MnO_2), J. Colloid Interface Sci. 330 (2009) 9–19.
[10] J. Tonkin, L. Balistrieri, J. Murray, Modeling sorption of divalent metal cations on hydrous manganese oxide using the diffuse double layer model, Appl. Geochem. 19 (2004) 29–53.
[11] C.L. Chen, X.K. Wang, Influence of pH, soil humic/fulvic acid, ionic strength and foreign ions on adsorption of thorium(IV) onto γ-Al_2O_3, Appl. Geochem. 22 (2007) 436–445.
[12] X.L. Tan, X.K. Wang, C.L. Chen, A.H. Sun, Effect of soil humic and fulvic acids, pH and ionic strength on Th(IV) sorption to TiO_2 nanoparticles, Appl. Radiat. Isotopes 65 (2007) 375–381.
[13] D. Xu, X.K. Wang, C.L. Chen, X. Zhou, X.L. Tan, Influence of soil humic acid and fulvic acid on adsorption of thorium(IV) on MX-80 betonite, Radiochim. Acta 94 (2006) 429–434.
[14] D. Xu, D.D. Shao, C.L. Chen, A.P. Ren, X.K. Wang, Effect of pH and fulvic acid on adsorption and complexation of cobalt onto bare and FA bound MX-80 bentonite, Radiochim. Acta 94 (2006) 97–102.
[15] G.D. Sheng, S.W. Wang, J. Hu, Y. Lu, J.X. Li, Y.H. Dong, X.K. Wang, Adsorption of Pb(II) on diatomite as affected via aqueous solution chemistry and temperature, Colloids Surf. A 339 (2009) 159–166.
[16] S.T. Yang, J.X. Li, Y. Lu, Y.X. Chen, X.K. Wang, Sorption of Ni(II) on GMZ bentonite: Effects of pH, ionic strength, foreign ions, humic acid and temperature, Appl. Radiat. Isotopes 67 (2009) 1600–1608.
[17] S.T. Yang, J.X. Li, D.D. Shao, J. Hu, X.K. Wang, Adsorption of Ni(II) on oxidized multi-walled carbon nanotubes: effect of contact time, pH, foreign ions and PAA, J. Hazard. Mater. 166 (2009) 109–116.
[18] X.L. Tan, X.K. Wang, H. Geckeis, T. Rabung, Sorption of Eu(III) on humic acid or fulvic acid bound to alumina studied by SEM-EDS, XPS, TRLFS and batch techniques, Environ. Sci. Technol. 42 (2008) 6532–6537.
[19] Z. Tao, J. Zhang, J. Zhai, Characterization and differentiation of humic acids and fulvic acids in soils from various regions of China by nuclear magnetic resonance spectroscopy, Anal. Chim. Acta 395 (1999) 199–203.
[20] J. Zhang, J. Zhai, F. Zhao, Z. Tao, Study of soil humic substances by cross-polarization magic angle spinning ^{13}C nuclear magnetic resonance and pyrolysis-capillary gas chromatography, Anal. Chim. Acta 378 (1999) 177–182.
[21] Y. Chin, G. Alken, E. O'Loughlin, Molecular weight, polydispersity, and spectroscopic properties of aquatic humic substances, Environ. Sci. Technol. 28 (1994) 1853–1858.
[22] Z. Li, Y. Ding, Y. Xiong, Y. Xie, Rational growth of various α-MnO_2 hierarchical structures and β-MnO_2 nanorods via a homogeneous catalytic route, Cryst. Growth Des. 5 (2005) 1953–1958.
[23] S. Liang, F. Teng, G. Bulgan, R. Zong, Y. Zhu, Effect of phase structure of MnO_2 nanorod catalyst on the activity for CO oxidation, J. Phys. Chem. C 112 (2008) 5307–5315.
[24] A. Vazquez-Olmos, R. Redon, G. Rodriguez-Gattorno, M. Mata-Zamora, F. Morales-Leal, A. Fernandez-Osorio, J. Saniger, One-step synthesis of Mn_3O_4 nanoparticles: structural and magnetic study, J. Colloid Interface Sci. 291 (2005) 175–180.
[25] D. Xu, X.L. Tan, C.L. Chen, X.K. Wang, Removal of Pb(II) from aqueous solution by oxidized multiwalled carbon nanotubes, J. Hazard. Mater. 154 (2008) 407–416.
[26] D. Xu, X.L. Tan, C.L. Chen, X.K. Wang, Adsorption of Pb(II) on MX-80 bentonite: effect of pH, ionic strength and temperature, Appl. Clay Sci. 41 (2008) 37–46.
[27] G.D. Sheng, J. Hu, X.K. Wang, Sorption properties of Th(IV) on the raw diatomite—effect of contact time, ionic strength and temperature, Appl. Radiat. Isotopes 66 (2008) 1313–1320.
[28] C. Weng, Modeling Pb(II) adsorption onto sandy loam soil, J. Colloid Interface Sci. 272 (2004) 262–270.
[29] C. Wu, Studies of the equilibrium and thermodynamics of the adsorption of Cu^{2+} onto as-produced and modified carbon nanotubes, J. Colloid Interface Sci. 311 (2007) 338–346.
[30] G. Pan, Y. Qin, X. Li, T. Hu, Z. Wu, Y. Xie, EXAFS studies on adsorption–desorption reversibility at manganese oxides–water interfaces I. Irreversible adsorption of zinc onto manganite (γ-MnOOH), J. Colloid Interface Sci. 271 (2004) 28–34.
[31] X. Li, G. Pan, Y. Qin, T. Hu, Z. Wu, Y. Xie, EXAFS studies on adsorption–desorption reversibility at manganese oxide–water interfaces II. Reversible adsorption of zinc on δ-MnO_2, J. Colloid Interface Sci. 271 (2004) 35–40.
[32] K. Hayes, J. Leckie, Modeling ionic strength effects on cation adsorption at hydrous oxide/solution interfaces, J. Colloid Interface Sci. 115 (1987) 564–572.
[33] G. Montavon, S. Markai, Y. Andres, B. Grambow, Complexation studies of Eu(III) with alumina-bound polymaleic acid: effect of organic polymer loading and metal ion concentration, Environ. Sci. Technol. 36 (2002) 3303–3309.
[34] Y. Takahashi, Y. Minai, S. Ambe, Y. Makide, F. Ambe, Comparison of adsorption behavior of multiple inorganic ions on kaolinite and silica in the presence of humic acid using the multitracer technique, Geochim. Cosmochim. Acta 63 (1999) 815–836.
[35] G.D. Sheng, D.D. Shao, Q.H. Fan, D. Xu, Y.X. Chen, X.K. Wang, Effect of pH and ionic strength on sorption of Eu(III) to MX-80 bentonite: batch and XAFS study, Radiochim. Acta 97 (2009) 621–630.
[36] I. Langmuir, The adsorption of gases on plane surfaces of glass, mica and platinum, J. Am. Chem. Soc. 40 (1918) 1361–1403.
[37] M. Kilpatrick, L. Baker Jr., C. McKinney Jr., Studies of fast reactions which evolve gases. The reaction of sodium–potassium alloy with water in the presence and absence of oxygen, J. Phys. Chem. 57 (1953) 385–390.
[38] Y.T. Zhou, H.L. Nie, C. Branford-White, Z.Y. He, L.M. Zhu, Removal of Cu^{2+} from aqueous solution by chitosan-coated magnetic nanoparticles modified with α-ketoglutaric acid, J. Colloid Interface Sci. 330 (2009) 29–37.
[39] M. Ajmal, R.A.K. Rao, S. Anwar, J. Ahmad, R. Ahmad, Adsorption studies on rice husk: removal and recovery of Cd(II) from wastewater, Bioresour. Technol. 86 (2003) 147–149.